ESTIMATION OF BOUNDARY SHAPE USING INVERSE METHOD IN A FUNCTIONALLY GRADED MATERIAL IN TWO DIMENSIONAL PROBLEM

Abbas Bazargani [1], Reza Amini [1], Mehdi Kashfi[1]

[1]Mr. CFD LLC., Tbilisi, Georgia

Abstract – *In this paper, conjugated gradient method (CGM) based inverse algorithm for transient heat conduction problem in a functionally graded material is performed to estimate the unknown boundary shape when measurement or observing the body shape is impossible or needs complex, accurate and expensive equipment. For example, when the unknown boundary placed in high temperature or unreachable environment. The governing equations are derived by using finite element method as a systematic and efficient theory. It is assumed that the material properties are smoothly changed based on mixture law. To determine the accuracy of the estimated data, problems with different boundary conditions, materials and boundary shapes was studied and all of them proved that the methods which was used in this paper, are completely compatible with the exact solution. Finally, the effect of parameters, such as the number of thermocouples, the measurement error, and volume fraction index and substituting the materials which was used in FGM stuff, was discussed and compared.*

Key words: Estimation of boundary shape; Inverse method; Functionally graded materials; Conjugate gradient method; finite element method; Inverse heat conduction problem(IHCP)

1. INTRODUCTION

Functionally graded materials (FGMs) are a new generation of composites which have found extensive applications in different industries because of their favorable and continuously varying physical and thermal properties [1–4]. Hence, these layered components are likely to play a great role in the construction of advanced structures, such as supersonic and hypersonic space vehicles and nuclear industries. Usually, these structural elements operate in a high temperature environment which inevitably induces some thermal stresses that can change their mechanical behavior [5–7] or cause a catastrophic failure of materials. Hence, an accurate and efficient determination of their thermal characteristic (boundary heat fluxes and temperature distributions) is of great interest for engineering design and manufacture. On the other hand, in some heat transfer problems the operational process for direct measurement of the physical parameters is either quite complicated or the measurement process corresponding to it requires sophisticated and expensive instruments. In such situations, satisfactory estimation results can be obtained using an inverse method in conjunction with simple instruments without disturbing the processes. For this purpose, transient temperature measurements taken at various boundary points of the body can be used for the estimation of the required quantities, and for this particular project the boundary shape. However, difficulties associated with the implementation of inverse analysis should also be recognized.

It is well-known that inverse problems are mathematically ill-posed; that is, a small change in the input data can result in enormous change in the computed solution at an inaccessible part of the boundary [8]. Hence, the inverse methods require efficient optimization tools for their solutions. The use of the adjoin equation approach coupled with the conjugate gradient method [9–14] appears to be very powerful for solving inverse heat conduction problems. In this method, the regularization procedure is performed during the iterative processes and thus, determination of optimal regularization conditions is not necessary.

The inverse heat conduction problem (IHCP) has been widely used in different practical engineering problems such as estimation of surface conditions, initial conditions, thermal properties and the boundary shape of a body, from known information at some predefined positions. For example, direct measurement or observing the boundary shape at the surface of a wall in general [15-18] and specifically subjected to fire, the outer surface of a vehicle re-entry or the inside surface of a combustion chamber is extremely difficult or needs expensive instruments [19]. Over the past decades, studies shows that numerical simulations [20-22] and experimental tests [23-25] have been consistence in different majors including heat transfer [26-30], energy [31], material [32-36], and other methods [37-40].

In the previous work by Huang and Chao a transient inverse geometry problem in identifying the unknown irregular boundary configurations from external measurements (either direct or infrared type) has been solved based on the boundary element method, i.e. In that work the boundary shape was a function of time. That approach could be applied to nondestructive evaluation (NDE) techniques and other such as the interface geometry identification for the phase change problems [41]. Kazemzade and Daneshmand also developed a shape identification scheme to determine the shape of the inaccessible parts of a 2-dimentional object made of functionally graded material using the measured temperatures on its accessible parts. They used the smoothed fixed grid finite element method which was a new approach based on the non-boundary-fitted meshes and the gradient smoothing technique were used for the solution of direct problem and shape sensitivity analysis. [42]

To the best of the authors' knowledge, there are few works on the inverse heat conduction analysis of FGMs [1, 2, 43–48]. This motivates us to consider the inverse transient heat conduction problems of 2 dimensional body shape made of FG material here. However, it should be mentioned that there are some valuable works on the inverse heat conduction analysis of isotropic materials; see, for example, references [49–55].

2. Mathematical modeling

The domain under consideration is a functionally graded plate that two side of the plate is isolated and the other two side is held in constant temperature which is represented in figure 1 (a) and also in figure 1 (b) placement of the ceramic and metal is shown. The unknown boundary shape is estimated by determining the temperature on the opposite side of the plate. Hence, we should first solve the direct problem.

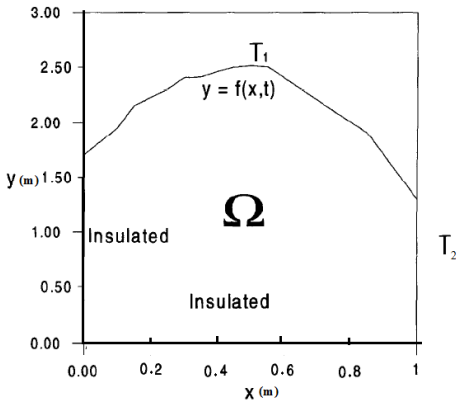

Fig. 1 (a): Geometry and the boundary condition, discussed in this paper.

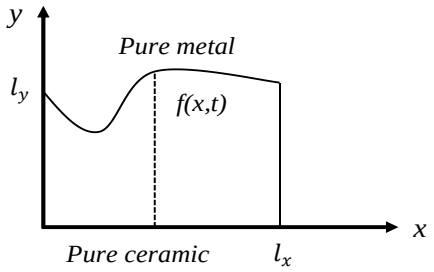

Fig. 1 (b): Placement of pure metal and ceramic on the boundary.

2.1 The direct problem

At the first step, we assume the unknown boundary shape as known. Then the temperature on the opposite side is determined due to it. For this purpose and to accurately do it, transient heat transfer equation without heat generation two-dimensional equation in FG materials is hired and the following equation is written as:

$$\frac{\partial}{\partial x}\left(k(y)\frac{\partial T}{\partial x}\right)+\frac{\partial}{\partial y}\left(k(y)\frac{\partial T}{\partial y}\right)=\rho(y)\,c(y)\frac{\partial T}{\partial t} \quad (1)$$

where $T\left[=T(x,y,t)\right]$, $\rho\left[=\rho(y)\right]$, $C\left[=C(y)\right]$ and $k\left[=k(y)\right]$ are respectively, temperature, mass density, specific heat capacity and thermal conductivity of an arbitrary material point of the plate.

The boundary and initial conditions are as follows, respectively,

$$\frac{\partial T(0,y)}{\partial x}=0 \quad (2)$$

$$\frac{\partial T(x,0)}{\partial y}=0 \quad (3)$$

$$T(l,y)=300k \quad (4)$$

$$T(x,f)=100k \quad (5)$$

$$T(x,y,0)=50k \quad (6)$$

The effective material properties of FG plate constituents (metal and ceramic) such as density (ρ), specific heat capacity (C) and thermal conductivity (k) are obtained by using the power law distribution, without loss of generality of the formulation and the method of solution. Hence, a typical effective material property 'G' is obtained as

$$G(y)=G_m(V_m)^n+G_c(V_c)^n \quad (7)$$

Where the subscripts c and m refer to the ceramic and metal constituents, respectively; also, $V_c\left(=\frac{y}{l_y}\right)$ is the volume fraction and n denotes the volume fraction index, which is a real positive number.

In this paper, finite element method (FEM) is applied to discretize the spatial differential equation as a systematic and efficient method. After finding the weak form for the equation number (1), applying by part integration and also using Green' theorem, the above equation is obtained:

$$\oint_{\Gamma^e}\left[k(y)w\frac{\partial T}{\partial x}n_x+k(y)w\frac{\partial T}{\partial y}n_y\right]ds=\oint_{\Gamma^e}wq_n\,ds \quad (8)$$

On the other side, in each element of the finite element meshes, we assume that:

$$T^e(x,y,t)=\sum_{i=1}^{n}T_e^i(t)N_i^e(x,y) \quad (9)$$

Shape function is shown as N_i^e, and also n is the number of nodes of the e-th element and T_e^i is temperature of the i-th node from the e-th element. Finally the governing equation will be:

$$\int_{\Omega^e}\left\{\begin{array}{l}\sum_{i=1}^{N}\left[k(y)\frac{\partial N_i}{\partial x}\frac{\partial N_j}{\partial x}+k(y)\frac{\partial N_i}{\partial y}\frac{\partial N_j}{\partial y}\right]T_j^e+\\ \sum_{j=1}^{N}(\rho c N_i N_j)\frac{\partial T_j^e}{\partial t}\end{array}\right\}dxdy-Q_e^i=0 \quad (10)$$

After assembling the element matrices and satisfying the boundary and initial condition, equation (10) changes to:

$$[K]\{T\}+[M]\{\dot{T}\}=\{Q\} \quad (11)$$

Where [K], [M] and {Q} are respectively hardness and mass matrix and force vector.

And also for time derivatives, backward finite difference method is used as an unconditionally stable method. After applying the method and rearranging the equation, the above equation is obtained:

$$\{T^{s+1}\}=([M]+\Delta t[K])^{-1}\times(\{Q\}\Delta t-[M]\{T^s\}) \quad (12)$$

where T^s is temperature in the s-th time step. Assuming the initial conditions and solving the above equation, quantity of the temperature for the next time step is obtained.

2.2. Creating elements and geometry of solvent procedure

Since the purpose of this paper is to estimate the boundary shape, the boundary shape changes in every time step. As a matter of fact, in every step the whole meshes should be terminated and rebuilt in the next time step [56-59]. Actually we're facing a moving mesh. On the other side, since the unknown boundary is curved shape, so the elements are irregular. For creating the matrices of hardness and mass and also the force vector, the irregular physical domain should be mapping to computational regular domain. As an efficient method for mapping the domain, the Gauss method is used. At this point, x and y direction changes to ξ and η

$$[g]=\begin{bmatrix}\frac{\partial x}{\partial \zeta} & \frac{\partial y}{\partial \zeta}\\ \frac{\partial x}{\partial \eta} & \frac{\partial y}{\partial \eta}\end{bmatrix}$$

$$\begin{bmatrix}\frac{\partial N_i}{\partial x}\\ \frac{\partial N_i}{\partial y}\end{bmatrix}=[G]\begin{bmatrix}\frac{\partial N_i}{\partial \zeta}\\ \frac{\partial N_i}{\partial \eta}\end{bmatrix} \quad (13)$$

$$[G]=[g]^{-1}$$

$$dxdy=(\det g)d\zeta d\eta$$

If N_i considers as shape function, the following equation is achieved:

$$K^e{}_{ij}=\int_{\Omega}\left(\frac{\partial N_i}{\partial x}\frac{\partial N_j}{\partial x}+\frac{\partial N_i}{\partial y}\frac{\partial N_j}{\partial y}\right)dxdy=$$
$$\int_{\Omega}\left[\begin{array}{l}\left(G_{11}^2+G_{21}^2\right)\frac{\partial N_i}{\partial \xi}\frac{\partial N_j}{\partial \xi}+\left(G_{12}^2+G_{22}^2\right)\frac{\partial N_i}{\partial \eta}\frac{\partial N_j}{\partial \eta}+\\ \left(G_{11}G_{12}+G_{21}G_{22}\right)\frac{\partial N_i}{\partial \xi}\frac{\partial N_j}{\partial \eta}+\left(G_{11}G_{12}+G_{21}G_{22}\right)\frac{\partial N_j}{\partial \xi}\frac{\partial N_i}{\partial \eta}\end{array}\right]\times (\det g)d\zeta d\eta \quad (14)$$

2.3 The inverse problem

In the inverse problem, the boundary shape is assumed to be unknown, while all the other effective parameters for solvent are known. Moreover, the temperature at some suitable locations on the other side of the plate in an arbitrary time t are considered to be available.

2.4 Sensitivity problem

The governing differential equations of the sensitivity problems are obtained from the original direct problem defined by Equations (1)-(6). For this purpose, perturbing $f(x,t)$ to $f(x,t)+\Delta f(x,t)$, then $T(x,t)$ change to $T(x,t)+\Delta T(x,t)$, respectively. Substituting these new values of the field variables in Equation (1) and neglecting the higher order terms, the governing differential equations of the sensitivity problems are obtained as

$$\frac{\partial}{\partial x}\left(k\frac{\partial(T+\Delta T)}{\partial x}\right)+\frac{\partial}{\partial y}\left(k\frac{\partial(T+\Delta T)}{\partial y}\right)=\rho c\frac{\partial(T+\Delta T)}{\partial t} \quad (15)$$

In a similar manner, the boundary conditions (2)-(6) become, respectively,

$$x=0:\frac{\partial \Delta T}{\partial x}=0 \quad (16)$$

$$x=l_x:\Delta T=0 \quad (17)$$

$$t=0:\Delta T=0 \quad (18)$$

$$y=0:\frac{\partial \Delta T}{\partial y}=0 \quad (19)$$

$$y=f(x,t):\Delta T=\Delta f\frac{\partial T}{\partial y} \quad (20)$$

2.5 Adjoin problem and gradient equation

In order to derive the governing differential equations of adjoin problem, Lagrange multipliers approach is adopted. Using this approach, the new functional is defined

$$\hat{J} = \int_{t=0}^{t_f}\int_{x=0}^{l}[T-Y]^2\,\delta(x-x_m)dxdt + \oint_{\Gamma}\lambda\left[\frac{\partial}{\partial x}\left(k\frac{\partial T}{\partial x}\right)+\frac{\partial}{\partial y}\left(k\frac{\partial T}{\partial y}\right)-\rho c\frac{\partial T}{\partial t}\right]dxdydt \quad (21)$$

In the adjoin problem, the values of the field variables are specified at the final time $t=t_j$ instead of the initial time t=0, as in the traditional initial value problems. However, by defining a new time variable as $(t_j - t)$, this problem is easily transformed to a standard initial value problem. Then, with perturbing $f(x,t)$ to $f(x,t)+\Delta f(x,t)$ and respectively $T(x,t)$ to $T(x,t)+\Delta T(x+t)$ and also by-parting the integration, the above equation is achieved:

$$\frac{\partial}{\partial x}\left(k\frac{\partial\lambda}{\partial x}\right)+\frac{\partial}{\partial y}\left(k\frac{\partial\lambda}{\partial y}\right)+\rho c\frac{\partial\lambda}{\partial t}=0 \quad (22)$$

And the boundary conditions become:

$$x=0 \;:\; \frac{\partial\lambda}{\partial x}=0 \quad (23)$$

$$x=l \;:\; \lambda=0 \quad (24)$$

$$y=0: \quad k\frac{\partial\lambda}{\partial y}=-2(T-Y)\delta(x-x_m) \quad (25)$$

$$t=t_j \;:\; \lambda=0 \quad (26)$$

$$y=f(x,t) \;:\; \lambda=0 \quad (27)$$

And the gradient of the above functional can be presented as:

$$\hat{J}'(x,t)=-k\frac{\partial\lambda}{\partial y}\frac{\partial T}{\partial y}\Big|_{y=f(x)} \quad (28)$$

2.6 conjugated gradient method for minimization

In this paper, for finding the temperature on the surface, the number of M thermocouple is placed on it. The thermocouples sense the temperature as $Y_m(t)$ which means the temperature for x_m in the time of t. $[Y_m(t)=Y(x_m,t)]$ the process of solving the inverse problem continues till the above functional minimizes:

$$J[f(x,t)]=\int_{t=0}^{t_f}\sum_{m=1}^{M}[T_m(t)-Y_m(t)]^2\,dt \quad (29)$$

In which $T_m(t)$ is known as the estimated temperature for x_m in the time of t. Based on the Conjugated gradient method, the unknown quantity $f(x,t)$ is estimated using an iterative process as follows,

$$f^{r+1}(x,t)=f^r(x,t)-\beta^r p^r(x,t), \quad (30)$$

r = 0,1,2,3, ...

Where β^r is the search step size in going from the iteration r to the iteration r+1 and $P^r(t)$ is the direction of descent (i.e. search direction) given by,

$$P^r(x,t)=\hat{J}'^r(x,t)+\gamma^r P^{r-1}(x,t), \quad (31)$$

Which is a conjugation of the gradient direction $\hat{J}'^r\left[=\left(\frac{\partial\hat{J}}{\partial f}\right)^r\right]$ at the iteration r and the direction of descent $P^{r-1}(t)$ at the iteration r-1. The conjugate coefficient (γ) at the iteration r is determined from the following relation,

$$\gamma^r=\frac{\int_0^{t_f}\int_0^{l_x}\left(\hat{J}'^r\right)^2dxdt}{\int_0^{t_f}\int_0^{l_x}\left(\hat{J}'^{r-1}\right)^2dxdt}, \quad (32)$$

$$\gamma^0=0$$

It can be seen that the method degenerate to the steepest descent method when $\gamma^r=0$ for any r in Eq. (31). The convergence of the above iterative procedure in minimizing the functional $\hat{J}$ is demonstrated previously [9].

After substituting the equation (30) in (29), the functional of $J(\hat{f}^{r+1})$ for iteration r+1 is written as bellow:

$$J\left[\hat{f}^{r+1}\right]=\int_{t=0}^{t_f}\sum_{m=1}^{M}\left[T_m\left(\hat{f}^{r}-\beta^r p^r\right)-Y_m(t)\right]^2 dt \quad (33)$$

After writing the derivation of the above equation toward β^r and also making it equivalent to zero, we reach to bellow equation as search step size:

$$\beta^r=\frac{\int_{t=0}^{t_f}\sum_{m=1}^{M}\left[T_m(t)-Y_m(t)\right]\Delta T_m(t)dt}{\int_{t=0}^{t_f}\sum_{m=1}^{M}\left[\Delta T_m^2(t)\right]dt} \quad (34)$$

2.7 Stopping criterion

The stopping criterion to terminate the iteration processes depends on the measurement errors. If the temperature at the surface can be measured accurately (i.e. without any measurement error) then as the value of the objective functional converge to a very small number, the computational procedure is stopped, i.e.

$$J\left[f^{r+1}(t)\right]<\varepsilon \quad (35)$$

where ε is a small specified number. But, since the measured temperature data contains some measurement errors, in this study the discrepancy principle is adopted as the stopping criterion to terminate the iteration procedure. Based on this criterion, the temperature residuals is approximated as,

$$\sigma\approx T_m(t)-Y_m(t) \quad (36)$$

Where σ is the standard deviation of the temperature measurements, which is assumed to be constant. Substituting Eq. (36) into Eq. (29), then the stopping criteria ε which should be used in inequality (35) is obtained as,

$$\varepsilon=M\sigma^2 t_j \quad (37)$$

2.8 Computational procedure

The computational procedure for the solution of this inverse problem using conjugate gradient method may be summarized as follows:

i. Set $f(x,t)$ as known for the first iteration

ii. Solve the direct problem given by equation (1)-(6) for $T(x,y,t)$

iii. Examine the stopping criterion given by equation (35) with ε given by equation (37). Continue if not satisfied

iv. Solve the adjoin problem given by equation (22)-(27) for $\lambda(x,y,t)$

v. Compute the gradient of the functional $\hat{J}'^r$ from equation(28)

vi. Compute the conjugate coefficient γ^r and direction of descent P^r from equation (32) and (31), respectively.

vii. Set $\Delta f=-p^r$, and solve the sensitivity problem given by equation (15)-(20) for $\Delta T(x,t)$

viii. Compute the search step size β^r from equation (34).

ix. Compute the new estimation for $f^{r+1}(x,t)$ from equation (30) and return to step II.

3. Numerical results and discussion

In this section, the accuracy of the proposed inverse algorithm in predicting the boundary shape on the functionally graded plate is investigated. For this purpose, 8 distinct example of FG plate with unknown boundary shapes are investigated. Also in this section the effect of parameters, such as the number of thermocouples, the measurement error, and volume fraction index and substituting the materials which was used in FGM stuff are discussed and compared with the exact solution. The number of thermocouples in the y-direction are the same as number of the nodes. The total time is assumed to be $t_f=40(s)$ and the value of $\Delta t=1(s)$ is used in all the solved examples. The material properties of the FG fins for different examples are presented in Table 1. Initial guess for the unknown boundary for all the examples is $f^0=0$.

Table 1 Thermo-physical properties of the materials.

Material	C(J/kgK)	k (W/mK)	ρ (kg/m3)
Iron	448	80	7850
Al2O3	775	30.7	3970
Aluminum	900	247	2712
Al2O3	775	30.7	3970

To compare the results for situations involving random measurement errors, the normally distributed uncorrelated errors with zero mean and constant standard deviation, σ, are used. The simulated vector of inexact measurement data Y can be expressed as

$$\{Y\}=\{Y_{exact}\}+\{\omega\} \quad (38)$$

where $\{Y\}$ represents the exact values of the temperature of the direct problem at different times and $\{\omega\}$ is the vector of random errors with zero mean and a specified standard

deviation. In all the solved examples, a value of $\varepsilon = 0.01$ is used for the case of $\sigma = 0$.

In the solved examples, the average error is evaluated based on the following formulation,

$$\%Error = \sum_{i=1}^{M}\sum_{j=1}^{J}\left|\frac{f(x_i,t_j) - \hat{f}(x_i,t_j)}{f(x_i,t_j)}\right| \div \left[M \times (J+1)\right] \times 100\% \quad (39)$$

In which $f(x_i,t_j)$ is the estimated equation for the unknown boundary shape and $\hat{f}(x_i,t_j)$ is the exact equation. And also M is the number of thermocouples in x-direction and J+1 is the number of time nodes.

For making sure that the method and the solvent process is correct, we compare the results with the Sakurai's results. [30] For this purpose, table 2 is shown.

Table 2. Comparison between results of Sukurai and this paper.

x	Present study	Sakurai (30)
0.1	7.865	7.863
0.2	6.231	6.226
0.3	4.911	4.901
0.4	3.658	3.652
0.5	2.695	2.691
0.6	1.934	1.928
0.7	1.247	1.238
0.8	0.836	0.831
0.9	0.421	0.416

The material which was used for the examples are Alumina as ceramic and Iron as metal, except example 64.

In the first and second example the equation of unknown boundary shapes are respectively, $y = 2 + x$ and $y = 1.5 + \sin(\pi x)$. Also $M = 20$ and $n = 2$. The estimated boundary shape for $\sigma = 0,0.5,1,3$ is shown and compared with the exact shape in figure 2 and 3. The computational time efforts and the percentage of average errors (evaluated using Eq. (39)) for the above solved examples are given in Table 3.

Table 3. The computational time efforts and percentage of errors for the first two examples.

σ		Example (1)	Example (2)
0.0	Number of iteration	14	22
	Error %	0.61	1.42
0.5	Number of iteration	8	14
	Error %	3.56	4.77
1	Number of iteration	11	8
	Error %	4.71	6.30
3	Number of iteration	6	11
	Error %	6.58	9.06

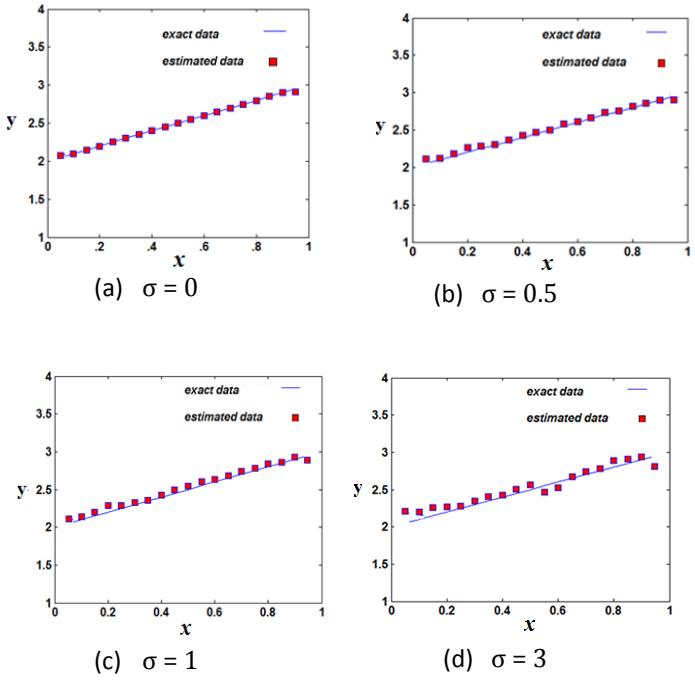

(a) σ = 0 (b) σ = 0.5

(c) σ = 1 (d) σ = 3

Fig. 2 (a)-(d): Comparison between the estimated and exact shape of boundary with equation $y = 2 + x$ for different standard deviation (example 1).

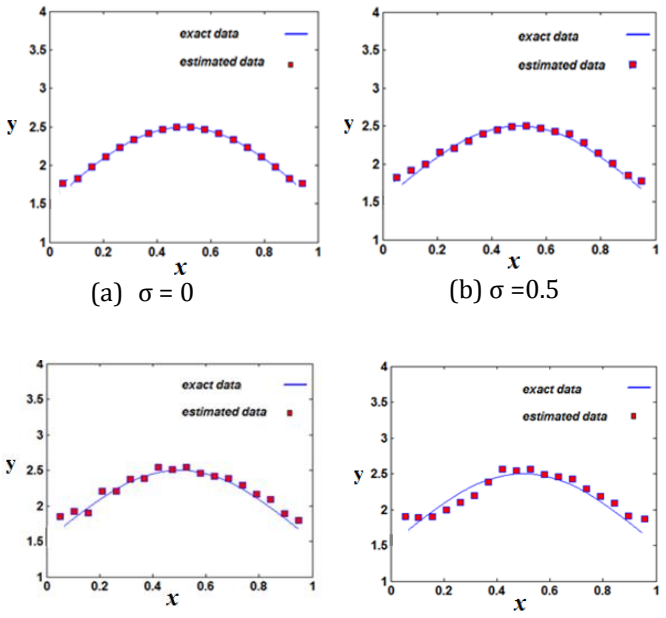

(a) σ = 0 (b) σ =0.5

(c) σ = 1 (d) σ = 3

Fig. 3 (a)-(d): Comparison between the estimated and exact shape of boundary with equation $y = 1.5 + \sin(\pi x)$ for different standard deviation (Ex. 2).

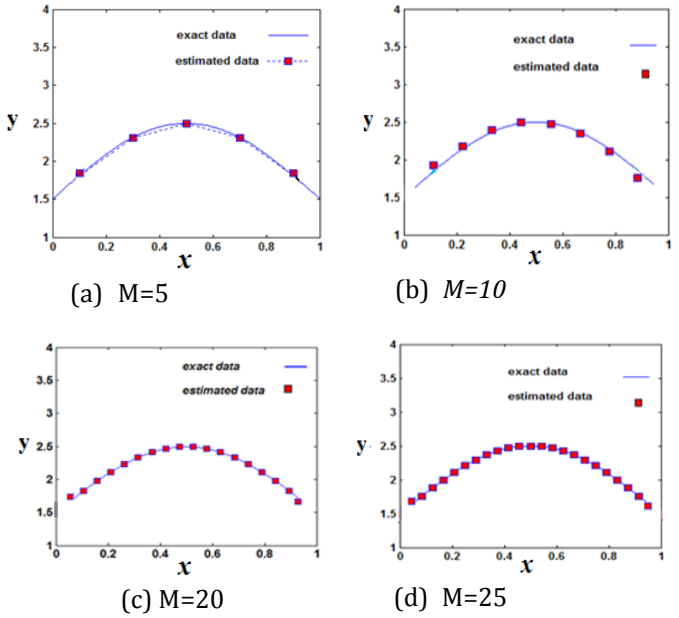

(a) M=5 (b) *M=10*

(c) M=20 (d) M=25

Fig. 4 (a)-(d): Comparison between the estimated and exact shape of boundary for different number of thermocouples with equation $y = 1.5 + \sin(\pi x)$ (Ex. 3).

In the third example, the effect of number of thermocouples is shown in figure 4 and discussed. The equation of unknown boundary shape is $y = 1.5 + \sin(\pi x)$ and also $\sigma = 0.2$ and $n = 2$. The purpose of this example is finding the thermocouple number, which has the minimum deviation with the exact answer.

In the fourth example, the effect of substituting the materials which was used in FGM stuff is discussed and compared in figure 5. The equation of unknown boundary shape is $y = 1.5 + 2x$ and also $\sigma = 0.2$ and $n = 2$. The purpose of this example is comparing the results when the place of the pure ceramic and metal is substituted.

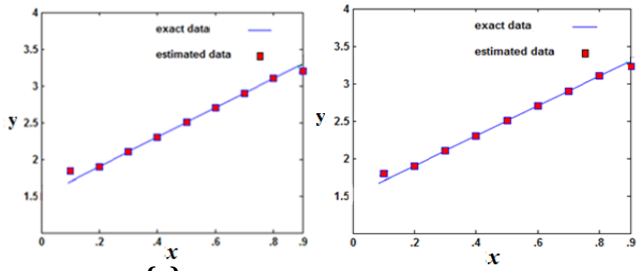

(a) **(b)**

Fig. 5 (a)-(b): Comparison between the estimated and exact shape of boundary with equation $y = 1.5 + 2x$ when a) metal is on y=0 (down) b) ceramic is on y=0 (down) (example 4).

In the fifth example, the effect of variable value for volume fraction index is presented in figure 6. The equation of unknown boundary shape is $y = 1.5 + \sin(2\pi x)$ and also $\sigma = 0.2$ and $M = 10$.

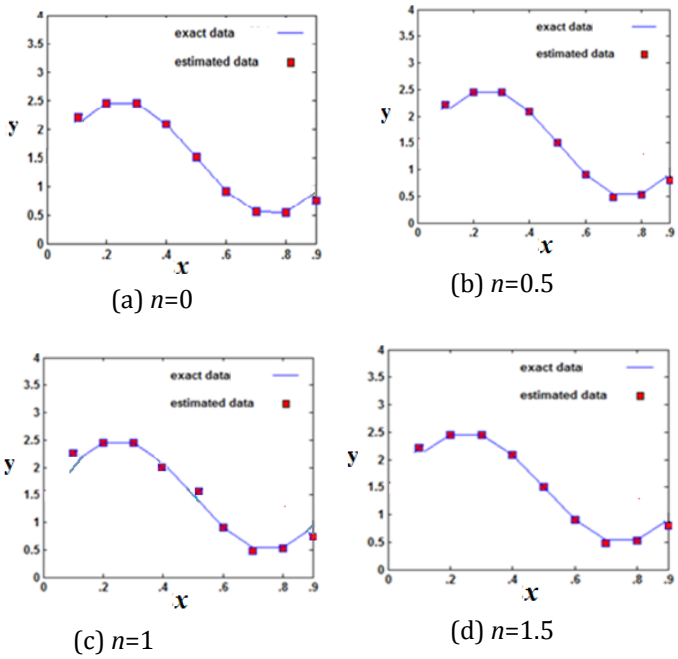

(a) *n*=0 (b) *n*=0.5

(c) *n*=1 (d) *n*=1.5

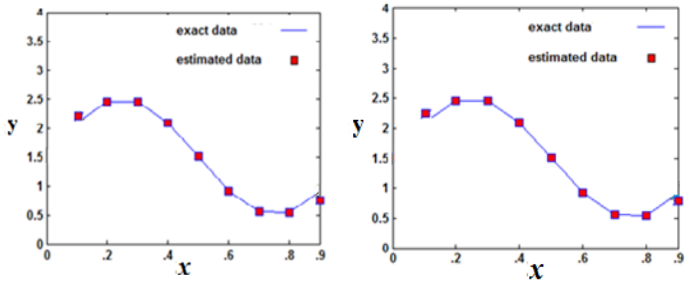

(e) n=3 (f) n=4

Fig. 6 (a)-(f): Comparison between the estimated and exact shape of boundary with equation $y = 1.5 + \sin(2\pi x)$ for various volume fraction indexes (example 5).

In the sixth example, different FG materials are used to compare the results. The equation of unknown boundary shape is $y = 1.5 + \sin(2\pi x)$ and also $\sigma = 0.2$ and $M = 10$. In the both figure 7 (a) and 7(b) Alumina is used as ceramic. Iron is used for the first part and Aluminum for the second part is hired as metal.

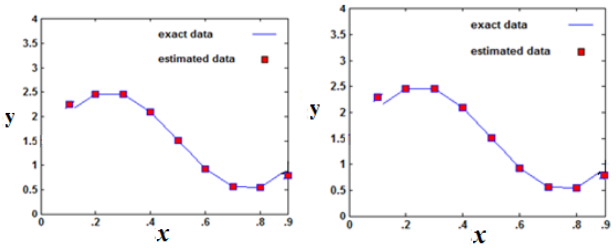

(a) (b)

Fig. 7 (a)-(b): Comparison between the estimated and exact shape of boundary with equation $y = 1.5 + \sin(2\pi x)$ when the FG plate consists of a) Iron and Alumina b) Aluminum and Alumina (example 6).

In the seventh and 8th example new boundary condition is performed, as figure 8 and also in the new boundary condition: $T = T_1 = 100$, $T = T_2 = 300$, $T = T_3 = 100$. The equation of unknown boundary shapes are respectively, $y = 2 + x$ and $y = 1.5 + \sin(\pi x)$. Also $M = 20$ and $n = 2$. The estimated boundary shape for $\sigma = 0$ is shown and compared with the exact figure in figure 9 and 10.

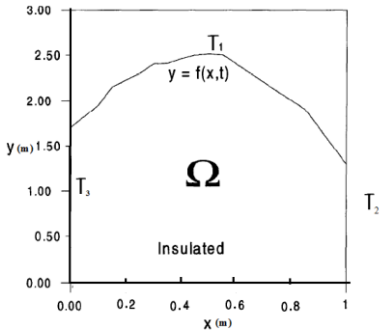

Fig. 8 Geometry and the boundary condition for example 7 and 8.

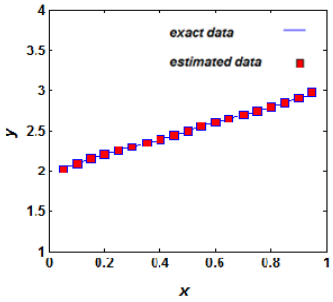

Fig. 9: Comparison between the estimated and exact shape of boundary with equation $y = 2 + x$ when $\sigma = 0$ for new boundary condition (example 7).

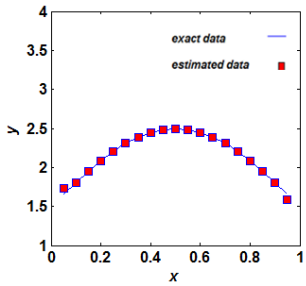

Fig. 10: Comparison between the estimated and exact shape of boundary with equation $y = 1.5 + \sin(\pi x)$ when $\sigma = 0$ for new boundary condition (example 8).

4. Conclusion

Inverse transient heat conduction problems of functionally graded (FG) plate is presented. The equation of boundary shape is estimated by using the measured temperature at the other side's plate. To accurately model the heat conduction phenomena, the non-Fourier heat transfer equation is used. The conjugate gradient method (CGM) is employed for the optimization procedure and the finite element method is applied to solve the governing differential equations. From the solved examples, it is revealed that the presented approach has the ability to predict the unknown boundary shape with good accuracy and low computational time efforts.

REFERENCES

[1] Haghighi, M.G., Eghtesad, M., Malekzadeh, P. and Necsulescu, D.S., 2008. Two-dimensional inverse heat transfer analysis of functionally graded materials in estimating time-dependent surface heat flux. Numerical Heat Transfer, Part A: Applications, 54(7), pp.744-762.

[2] Haghighi, M.G., Eghtesad, M., Malekzadeh, P. and Necsulescu, D.S., 2009. Three-dimensional inverse transient heat transfer analysis of thick functionally graded plates. Energy conversion and management, 50(3), pp.450-457.

[3] Haghighi, M.G., Eghtesad, M., Necsulescu, D.S. and Malekzadeh, P., 2010. Temperature control of functionally graded plates using a feedforward–feedback controller based on the inverse solution and proportional-derivative controller. Energy Conversion and Management, 51(1), pp.140-146.

[4] Marin, L. and Lesnic, D., 2007. The method of fundamental solutions for nonlinear functionally graded materials. International journal of solids and structures, 44(21), pp.6878-6890.

[5] Malekzadeh, P., Haghighi, M.G. and Atashi, M.M., 2010. Out-of-plane free vibration of functionally graded circular curved beams in thermal environment. Composite Structures, 92(2), pp.541-552.

[6] Malekzadeh, P., 2009. Two-dimensional in-plane free vibrations of functionally graded circular arches with temperature-dependent properties. Composite Structures, 91(1), pp.38-47.

[7] Farid, M., Zahedinejad, P. and Malekzadeh, P., 2010. Three-dimensional temperature dependent free vibration analysis of functionally graded material curved panels resting on two-parameter elastic foundation using a hybrid semi-analytic, differential quadrature method. Materials & Design, 31(1), pp.2-13.

[8] J. V. Beck, B. Blackwell, C. R. St., 1985. Clair, Inverse Heat Conduction, Wiley, New York.

[9] Alifanov, O.M., 1974. Solution of an inverse problem of heat conduction by iteration methods. Journal of Engineering Physics and Thermophysics, 26(4), pp.471-476.

[10] Alifanov, O.M., Artiūkhin, E.A. and Rumiāntsèv, S.V., 1995. Extreme methods for solving ill-posed problems with applications to inverse heat transfer problems. New York: Begell house.

[11] Ozisik, M. Necat. Inverse heat transfer: fundamentals and applications. Routledge, 2018.

[12] Woodbury, K.A., 2002. Inverse engineering handbook. Crc press.

[13] Jarny, Y., Ozisik, M.N. and Bardon, J.P., 1991. A general optimization method using adjoint equation for solving multidimensional inverse heat conduction. International journal of heat and mass transfer, 34(11), pp.2911-2919.

[14] Huang, C.H. and Wang, S.P., 1999. A three-dimensional inverse heat conduction problem in estimating surface heat flux by conjugate gradient method. International Journal of Heat and Mass Transfer, 42(18), pp.3387-3403.

[15] Razavi, A. and Sarkarb, P.P., 2016. Laboratory investigation of the effect of tornado translation on its near-ground flow field. Laboratory investigation.

[16] Razavia, A. and Sarkar, P.P., 2018. Laboratory investigation of the effects of translation on the near-ground tornado flow field. Wind and Structures, 26(3), pp.179-190.

[17] Razavi, A. and Sarkar, P.P., 2018. Laboratory Study of Topographic Effects on the Near-surface Tornado Flow Field. Boundary-Layer Meteorology, pp.1-24.

[18] Razavi, A., 2018. Laboratory study of parameters influencing tornado flow field and tornado loading on low-rise buildings. https://lib.dr.iastate.edu/etd/16660

[19] Haghighi, M.G., Eghtesad, M., Malekzadeh, P. and Necsulescu, D.S., 2009. Three-dimensional inverse transient heat transfer analysis of thick functionally graded plates. Energy conversion and management, 50(3), pp.450-457.

[20] Babajani, A.A., Jafari, M. and Sefat, P.H., 2016. Numerical investigation of distance effect between two Searasers for hydrodynamic performance. Alexandria Engineering Journal, 55(3), pp.2257-2268.

[21] Jafari, M., Soioudi, A. and Hafezisefat, P., 2017. Numerical Study of Aeroacoustic Sound on Performance of Bladeless Fan. Chinese Journal of Mechanical Engineering, 30(2), pp.483-494.

[22] Jafari, M., Babajani, A., Hafezisefat, P., Mirhosseini, M., Rezania, A. and Rosendahl, L., 2018. Numerical simulation of a novel ocean wave energy converter. Energy Procedia, 147, pp.474-481.

[23] Haghighat, A.K., Roumi, S., Madani, N., Bahmanpour, D. and Olsen, M.G., 2018. An intelligent cooling system and control model for improved engine thermal management. Applied Thermal Engineering, 128, pp.253-263.

[24] Atefi, G.A., Jafari, M.M., Khalesi, J. and Solevmani, A., 2010. The thermoelastic analysis of a gas turbine blade in 2-D and temperature dependent mechanical properties. In 9th Iranian Aero. Soci. Conf., Azad Univ. of Science and Research.

[25] Khaleghi, H., Dehkordi, M.A.S. and Tousi, A.M., 2016. Role of tip injection in desensitizing the compressor to the tip clearance size. Aerospace Science and Technology, 52, pp.10-17.

[26] Moheimani, R. and Hasansade, M., 2018. A closed-form model for estimating the effective thermal conductivities of carbon nanotube–polymer nanocomposites. Proceedings of the Institution of Mechanical Engineers, Part C: Journal of Mechanical Engineering Science, p.0954406218797967.

[27] Khalesi, J., Modaresahmadi, S. and Atefi, G., 2018. SEM Gamma prime observation in a thermal and stress analysis of a first-stage Rene'80H gas turbine blade: numerical and experimental investigation. Iranian Journal of Science and Technology, Transactions of Mechanical Engineering, pp.1-14.

[28] Damadam, M., Moheimani, R. and Dalir, H., 2018. Bree's diagram of a functionally graded thick-walled cylinder under thermo-mechanical loading considering nonlinear kinematic hardening. Case Studies in Thermal Engineering, 12, pp.644-654.

[29] Atefi, G.A., Jafari, M.M., Solevmani, A. and Khalesi, J., 2010. Analysis of flow and temperature field on turbine

blade with temperature dependent heat conduction coefficient. In 9th Iranian Aero. Soci. Conf., Azad Univ. of Science and Research.

[30] Hafezisefat, P., Esfahany, M.N. and Jafari, M., 2017. An experimental and numerical study of heat transfer in jacketed vessels by SiO2 nanofluid. Heat and Mass Transfer, 53(7), pp.2395-2405.

[31] Aminzahed, I., Zhang, Y. and Jabbari, M., 2016. Energy harvesting from a five-story building and investigation of frequency effect on output power. International Journal on Interactive Design and Manufacturing (IJIDeM), 10(3), pp.301-308.

[32] Moheimani, R., Damadam, M., Nayebi, A. and Dalir, H., 2018. Thick-Walled Functionally Graded Material Cylinder under Thermo-Mechanical Loading. In 2018 9th International Conference on Mechanical and Aerospace Engineering (ICMAE) (pp. 505-510). IEEE.

[33] Modaresahmadi, S., Li, K., Williams, W.B. and Bird, J.Z., 2018, April. Vibration Analysis of the First Stage of a Multi-stage Coaxial Magnetic Gearbox. In SoutheastCon 2018 (pp. 1-8). IEEE.

[34] Modaresahmadi, S., Li, K., Williams, W.B. and Bird, J.Z., 2018, April. Vibration Analysis of the First Stage of a Multi-stage Coaxial Magnetic Gearbox. In SoutheastCon 2018 (pp. 1-8). IEEE.

[35] Modares Ahmadi, S., Ghazavi, M. and Sheikhzad, M., 2015. Dynamic analysis of a rotor supported on ball bearings with waviness and centralizing springs and squeeze lm dampers. International Journal of Engineering, 28, pp.1351-1358.

[36] Moheimani, R. and Ahmadian, M.T., 2012. On Free Vibration of Functionally Graded Euler-Bernoulli Beam Models Based on the Non-Local Theory. In ASME 2012 International Mechanical Engineering Congress and Exposition (pp. 169-173). American Society of Mechanical Engineers.

[37] Aminzahed, I., Mashhadi, M.M. and Sereshk, M.R.V., 2017. Investigation of holder pressure and size effects in micro deep drawing of rectangular work pieces driven by piezoelectric actuator. Materials Science and Engineering: C, 71, pp.685-689.

[38] Varyani, A., Jalilvand-Nejad, A. and Fattahi, P., 2014. Determining the optimum production quantity in three-echelon production system with stochastic demand. The International Journal of Advanced Manufacturing Technology, 72(1-4), pp.119-133.

[39] Esmaili Torshabi, A. and Ghorbanzadeh, L., 2017. A Study on Stereoscopic X-ray Imaging Data Set on the Accuracy of Real-Time Tumor Tracking in External Beam Radiotherapy. Technology in cancer research & treatment, 16(2), pp.167-177.

[40] Ghorbanzadeh, L., Torshabi, A.E., Nabipour, I.S. and Arbatan, M.A., 2016. Development of a synthetic adaptive neuro-fuzzy prediction model for tumor motion tracking in external radiotherapy by evaluating various data clustering algorithms. Technology in cancer research & treatment, 15(2), pp.334-347.

[41] Huang, C.H. and Tsai, C.C., 1998. A transient inverse two-dimensional geometry problem in estimating time-dependent irregular boundary configurations. International Journal of Heat and Mass Transfer, 41(12), pp.1707-1718.

[42] Kazemzadeh-Parsi, M.J. and Daneshmand, F., 2013. Inverse geometry heat conduction analysis of functionally graded materials using smoothed fixed grid finite elements. Inverse Problems in Science and Engineering, 21(2), pp.235-250.

[43] Turteltaub, S., 2002. Functionally graded materials for prescribed field evolution. Computer Methods in Applied Mechanics and Engineering, 191(21-22), pp.2283-2296.

[44] Marin, L., 2005. Numerical solution of the Cauchy problem for steady-state heat transfer in two-dimensional functionally graded materials. International Journal of Solids and Structures, 42(15), pp.4338-4351.

[45] Sladek, J., Sladek, V. and Hon, Y.C., 2006. Inverse heat conduction problems by meshless local Petrov–Galerkin method. Engineering Analysis with Boundary Elements, 30(8), pp.650-661.

[46] Marin, L., 2009. Boundary reconstruction in two-dimensional functionally graded materials using a regularized MFS. Computer Modeling in Engineering and Sciences (CMES), 46(3), p.221.

[47] Sladek, J., Sladek, V., Wen, P.H. and Hon, Y.C., 2009. The inverse problem of determining heat transfer coefficients by the meshless local Petrov-Galerkin method. Computer Modeling in Engineering and Sciences (CMES), 48(2), p.191.

[48] Chang, W.J., Lee, H.L. and Yang, Y.C., 2011. Estimation of heat flux and thermal stresses in functionally graded hollow circular cylinders. Journal of Thermal Stresses, 34(7), pp.740-755.

[49] Huang, C.H. and Wu, H.H., 2006. An iterative regularization method in estimating the base temperature for non-Fourier fins. International journal of heat and mass transfer, 49(25-26), pp.4893-4902.

[50] Huang, C.H., Hsu, G.C. and Jang, J.Y., 2001. A nonlinear inverse problem for the prediction of local thermal contact conductance in plate finned-tube heat exchangers. Heat and mass transfer, 37(4-5), pp.351-359.

[51] Hsu, P.T. and Chu, Y.H., 2004. An inverse non-Fourier heat conduction problem approach for estimating the boundary condition in electronic device. Applied Mathematical Modelling, 28(7), pp.639-652.

[52] Wang, C.C., 2010. Direct and inverse solutions with non-Fourier effect on the irregular shape. International Journal of Heat and Mass Transfer, 53(13-14), pp.2685-2693.

[53] Yang, C.Y., 2009. Direct and inverse solutions of the two-dimensional hyperbolic heat conduction problems. Applied Mathematical Modelling, 33(6), pp.2907-2918.

[54] Hsu, P.T., 2006. Estimating the boundary condition in a 3D inverse hyperbolic heat conduction problem. Applied Mathematics and Computation, 177(2), pp.453-464.

[55] Sakurai, H., 2009. Transient and steady-state heat conduction analysis of two-dimensional functionally graded materials using particle method. WIT Transactions on Engineering Sciences, 64, pp.45-54.

[56] Feng, B., Levitas, V.I. and Kamrani, M., 2018. Coupled strain-induced alpha to omega phase transformation and plastic flow in zirconium under high pressure torsion in a rotational diamond anvil cell. Materials Science and Engineering: A.

[57] Kamrani, M., Levitas, V.I. and Feng, B., 2017. FEM simulation of large deformation of copper in the quasi-constrain high-pressure-torsion setup. Materials Science and Engineering: A, 705, pp.219-230.

[58] Kamrani, M., Feng, B. and Levitas, V.I., 2018. Modeling of Strain-Induced Phase Transformations Under High Pressure and Shear. In Proceedings of the International Conference on Martensitic Transformations: Chicago (pp. 47-51). Springer, Cham.

[59] Kamarni, M. and Kadkhodaei, M., 2014. An investigation into the simple tensile test of SMA wires considering stress concentration of grippers. Journal of materials engineering and performance, 23(3), pp.1114-1123.